Chapter 2
The Hodgkin–Huxley Theory of Neuronal Excitation

Hodgkin and Huxley (1952) proposed the famous Hodgkin–Huxley (hereinafter referred to as HH) equations which quantitatively describe the generation of action potential of squid giant axon, although there are still arguments against it (Connor et al. 1977; Strassberg and DeFelice 1993; Rush and Rinzel 1995; Clay 1998). The HH equations are important not only in that it is one of the most successful mathematical model in quantitatively describing biological phenomena but also in that the method (the *HH formalism* or the *HH theory*) used in deriving the model of a squid is *directly applicable* to many kinds of neurons and other excitable cells. The equations derived following this HH formalism are called the *HH-type equations*.

The dynamical system theory is very useful to analyze and understand the dynamics of the HH equations. On the other hand, the HH equations have rich mathematical structures and give many insights to mathematics also. For example, there are still many studies and mathematical findings on the "classical" HH equations (Plant 1976; Rinzel 1978; Hassard 1978; Troy 1978; Rinzel and Miller 1980; Labouriau 1985, 1989; Hassard and Shiau 1989; Shiau and Hassard 1991; Bedrov et al. 1992; Guckenheimer and Labouriau 1993; Labouriau and Ruas 1996; Fukai et al. 2000a,b). This chapter gives an overview of the dynamics of the HH equations and of the mechanism of the action potential generation.

2.1 What is a Neuron? Neuron is a Signal Converter

Figure 2.1 illustrates a shape and a function of neurons schematically. Our brain is a complicated network of a tremendous number of *neurons*. Right figure shows a *small* network of three neurons. A neuron has a very special shape which is much different from usual sphere-shaped or disklike cells. A *soma* is the main body of neuron from which a long cable called an *axon* is extended. Neurons transmit and exchange electric signals called *action potentials* or *spikes*, each other. (The generation of a spike is also called as the *excitation* or the *firing* of a neuron.) Neurons receive the spikes at a *synapse* which is a connection between neurons. Then, the electric signals or information is transmitted in the direction from a *dendrite* to an axon. The upper-left panel of Fig. 2.1 illustrates the waveform of action potentials. Action potential or a spike has an amplitude of about 100 mV.

S. Doi et al., *Computational Electrophysiology*,
DOI 10.1007/978-4-431-53862-2_2,

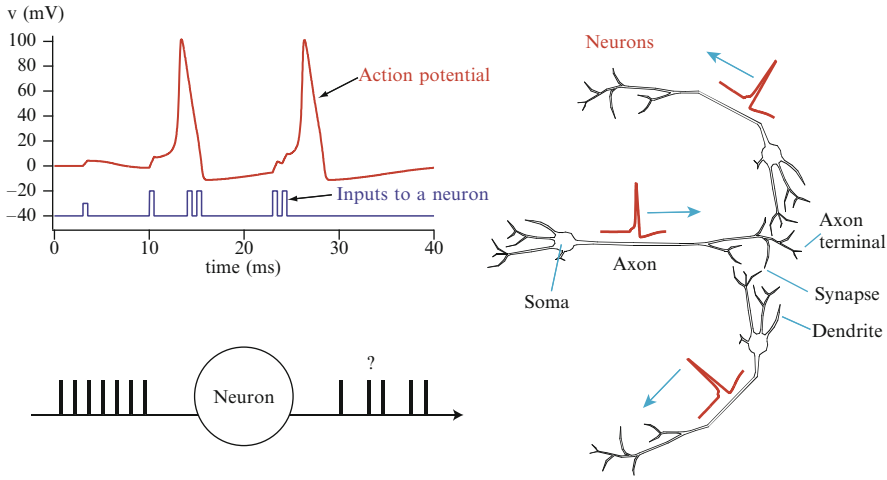

Fig. 2.1 Diagrams illustrating: A network of three neurons which exchange electric signals called action potentials, each other (*right*). Waveform of action potentials (*upper left*). Neuron as a device which converts input signals to output signals (*lower left*)

Typical neurons do not generate any spikes without input signals (i.e. spikes from other neurons). A sufficiently large input pulse causes a neuron to generate an output spike, as illustrated in the upper-left panel, whereas no output spike is generated by a small input (the first pulse in the lower trace of the upper-left panel). Therefore, a neuron possesses a *threshold* or *all-or-none* characteristic. There is a special period or timing called the *refractory period* (the timing of the downstroke of the action potential) in which the neuron cannot produce any output spike even though sufficient amount of inputs (the third and fourth pulses in the panel) were put in the neuron. Thus, we can consider a neuron as a device which transforms or converts the train of input spikes to a train of output spikes (see the lower-left panel of Fig. 2.1).

2.2 The Hodgkin–Huxley Formulation of Excitable Cell Membranes

This section briefly explains the framework of the HH formalism to model the action potential generation of neurons and of other excitable cells.

Biological cells, including neurons, are enclosed by a *plasma membrane* or simply *membrane* which separates the intracellular and extracellular water-containing media. The cell membrane consists of lipid bilayer, as shown in Fig. 2.2. There are various ions in both the intra- and extra-cellular regions. The concentrations of ions, however, are much different between the intra- and extra-cellular regions. For example, the concentration of K^+ ion is high and low in the intra- and extra-cellular regions, respectively. On the contrary, that of Na^+ ion is low and high

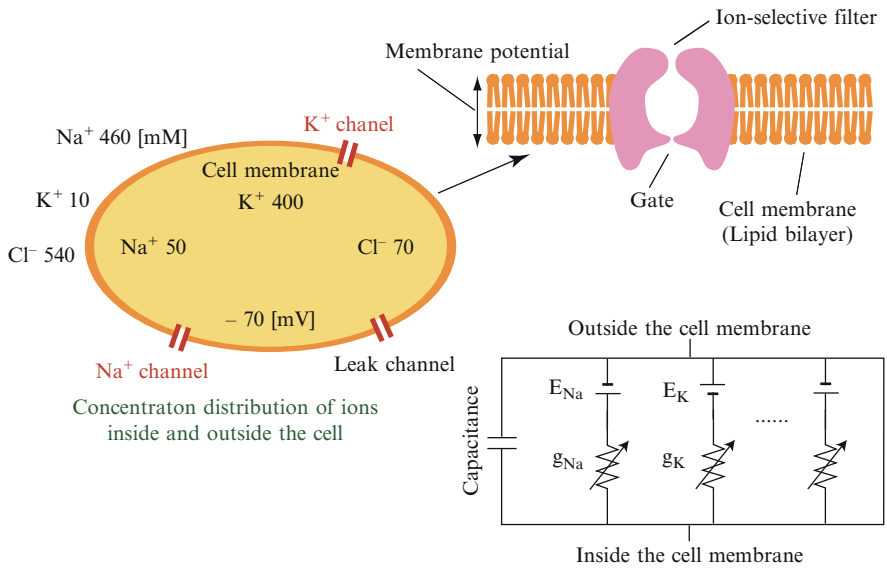

Fig. 2.2 The equivalent-circuit formulation of a cell membrane and ionic channels by Hodgkin and Huxley

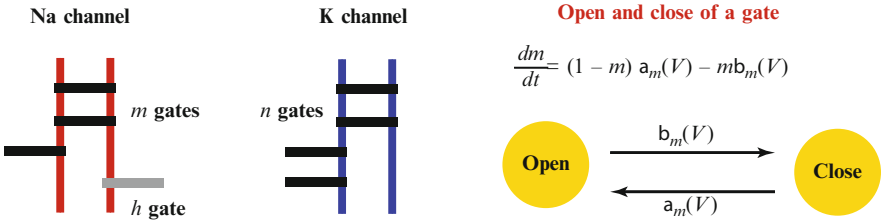

Fig. 2.3 Diagrams explaining the gate dynamics

in the intra- and extra-cellular regions, respectively. Usually, the resistance of the membrane is very high and the membrane acts as an insulator to the movement of ions. If the electrical potential at the inside surface of the cell membrane is compared to the potential at the outside surface, there is a potential difference or voltage called the *transmembrane potential* or simply the *membrane potential*.

In the membrane, there are holes through which ions can move in and out. Such a hole is called an *ion channel* and consists of *membrane proteins*. Ion channels are not simple holes (pores) or passive resistors through which ion flux flows. Ion channels are selective for a particular ion. For example, an ionic channel named Na^+ channel can pass only Na^+ ions. Also, ion channels are dynamic and sensitive to the membrane potential and to other factors. Namely, they open and close depending on such factors. An ion channel has several *gates* and the opening and closing of the ion channel are controlled by the gates as shown in Fig. 2.3. Note that, there

are various types of ionic channels which pass a specific ion. Particularly, there are many variants of K^+ channels classified by their various characteristics (Adams 1982; Crill and Schwindt 1983; Llinas 1988; Hille 1992).

The basic idea of the HH formalism is to just recognize the cell membrane as a simple electric circuit as shown in the lower-right panel of Fig. 2.2. The capacitive property of the cell membrane is denoted by the *capacitor* with a certain *capacitance* in the circuit. Na^+ and K^+ channels are modeled by the *resistors* which have *conductances* g_{Na} and g_K, respectively. Note that the resistors are not linear but nonlinear, and also are dynamic: the values of the conductances vary temporally, which are explained later. There is a tendency that Na^+ ions flow inward and that K^+ ions flow outward the cell membrane because there are differences in the concentrations of the ions between inside and outside of the membrane. Namely, ions have a tendency to move down their concentration gradients. Such a tendency is denoted by the batteries with voltages E_{Na} and E_K in the circuit. These voltages depend on the inside–outside concentration difference in each ion. Notice that the polarities of the batteries E_{Na} and E_K are reversed.

2.3 Nonlinear Dynamical Analysis of the Original HH Equations

The Hodgkin–Huxley equations (Hodgkin and Huxley 1952) of a squid giant axon are simply the differential equations of the electric circuit shown in Fig. 2.2 and are described as follows:

$$C\frac{\partial v}{\partial t} = \frac{a}{2\rho}\frac{\partial^2 v}{\partial x^2} + G(v,m,n,h) + I_{\text{ext}}, \tag{2.1a}$$

$$\frac{\partial m}{\partial t} = \alpha_m(v)(1-m) - \beta_m(v)m, \tag{2.1b}$$

$$\frac{\partial n}{\partial t} = \alpha_n(v)(1-n) - \beta_n(v)n, \tag{2.1c}$$

$$\frac{\partial h}{\partial t} = \alpha_h(v)(1-h) - \beta_h(v)h; \tag{2.1d}$$

$$\begin{aligned} G(v,m,n,h) &= I_{Na}(v,m,h) + I_K(v,n) + I_L(v) \\ &= \bar{g}_{Na}m^3h(V_{Na}-v) + \bar{g}_K n^4(V_K - v) + \bar{g}_L(V_L - v); \end{aligned} \tag{2.2}$$

$C = 1\,\mu\text{F}\,\text{cm}^{-2}$, $\bar{g}_{Na} = 120\,\text{mS}\,\text{cm}^{-2}$, $\bar{g}_K = 36\,\text{mS}\,\text{cm}^{-2}$, $\bar{g}_L = 0.3\,\text{mS}\,\text{cm}^{-2}$,
$V_{Na} = 115\,\text{mV}$, $V_K = -12\,\text{mV}$, $V_L = 10.599\,\text{mV}$;

$$\alpha_m(v) = \frac{0.1(25-v)}{\exp[(25-v)/10]-1}, \quad \beta_m(v) = 4e^{-v/18},$$
$$\alpha_n(v) = \frac{0.01(10-v)}{\exp[(10-v)/10]-1}, \quad \beta_n(v) = 0.125e^{-v/80},$$
$$\alpha_h(v) = 0.07\exp[-v/20], \quad \beta_h(v) = \frac{1}{\exp[(30-v)/10]+1};$$

where v (mV) is the membrane potential. Equation (2.1a) simply denotes the Kirchhoff's law. (In (2.1), a neuron is considered as a cylinder-shaped cell and the dependence of v on its position x is also taken into account. The term $(a/2\rho)(\partial^2 v/\partial x^2)$ denotes the diffusions of ions along the axis of the cylinder. However, either the shape of neurons or the x-dependence are not considered in this book.) $I_{\rm Na}$ and $I_{\rm K}$ are the currents through Na^+ and K^+ channels, respectively. The current $I_{\rm L}$ is the leak current and denotes all residue currents through a cell membrane other than Na^+ and K^+ currents.

As seen from (2.2), the Na^+ current $I_{\rm Na}$ is denoted by $\bar{g}_{\rm Na}m^3h(V_{\rm Na}-v)$ which takes a form of (*Conductance*) $\times$ (*Voltage*): Ohm's law. The voltage $V_{\rm Na}$ is called the *Nernst potential* or the *equilibrium potential* or sometimes the *resting potential* (do not confuse with the resting potential of whole membrane) of Na^+ ion. The Nernst potential is the potential where the tendency of ions to move down their concentration gradient is exactly balanced with the force by the electric potential difference; no Na^+ current flow through the Na^+ channel when $v = V_{\rm Na}$. $\bar{g}_{\rm Na}m^3h$ $(= g_{\rm Na}$ in the circuit of Fig. 2.2) denotes the conductance of Na^+ channel where the constant $\bar{g}_{\rm Na}$ is called the *maximum conductance* of the channel and m^3h denotes dynamic or temporal change of the conductance. In the K^+ current $I_{\rm K}$, the term n^4 denotes the temporal change of K^+ channel conductance.

The variables m, n and h take a (dimensionless) value between zero and unity, and are called the *gate variables*. As seen from the left panel of Fig. 2.3, it is assumed that Na^+ channel possesses three m-gates and single h-gate whereas K^+ channel four n-gates. In the HH formalism, it is also assumed that the variables m, n and h denote the probabilities that corresponding gates are open. The dynamic opening and closing of gates obey a simple (linear) process described by (2.1b–d) where $\alpha_m(v)$ ($\beta_m(v)$) is the rate "constant" for changing from closed (opened) state to opened (closed, resp.) state, as shown in the right panel of Fig. 2.3. Note that the rate "constant" $\alpha_m(v)$ and $\beta_m(v)$ are not actually the constants but the functions which depend on the membrane potential v. m and h are also called the activation and inactivation variables of Na^+ ionic channel, respectively, while n the activation variable of K^+ channel. The reason of this naming is because m and n are the increasing functions of v while h the decreasing one. $I_{\rm ext}$ (μA cm^{-2}) is the constant current externally applied to a neuron. The constants a and ρ are the radius and resistivity of the "cylindrical" axon, respectively. Throughout this book, we do not treat either such a cylindrical axon or the partial differential equation (2.1) which is an *infinite-dimensional* dynamical system. For the rich and complicated dynamics of such neuronal cable equations, see Carpenter (1977), Horikawa (1994), Kepler and Marder (1993), Rinzel and Keener (1983), Poznanski (1998), and Yanagida (1985, 1987, 1989).

2.3.1 Simple Dynamics of Gating Variables

In the following, we assume that the membrane potential v is spatially constant and omit the spatial derivative in (2.1); we consider the following HH equations for a *space-clamped* squid giant axon:

$$C\frac{dv}{dt} = G(v,m,n,h) + I_{\text{ext}}, \tag{2.3a}$$

$$\frac{dm}{dt} = \frac{1}{\tau_m(v)}(m^\infty(v) - m), \tag{2.3b}$$

$$\frac{dn}{dt} = \frac{1}{\tau_n(v)}(n^\infty(v) - n), \tag{2.3c}$$

$$\frac{dh}{dt} = \frac{1}{\tau_h(v)}(h^\infty(v) - h), \tag{2.3d}$$

where

$$\tau_x(v) = \frac{1}{\alpha_x(v) + \beta_x(v)}, \quad x^\infty(v) = \frac{\alpha_x(v)}{\alpha_x(v) + \beta_x(v)}, \quad x = m,n,h. \tag{2.4}$$

(The word "space-clamped" means that both the shape of a neuron and the dependence of the membrane potential v on the spacial position x are ignored while both were taken into account in (2.1).)

Figure 2.4 shows an example of a numerically solved solution of the HH equations (2.3). Panel (a) is a waveform of the membrane potential. A pulsatile input applied at a time $t = 5$ ms induces an action potential. Panel (b) is the waveforms of the gating variables m, n and h. Total membrane current, Na current, K current and leak current are shown in (c)–(f), respectively.

The HH equations (2.3) are nonlinear differential equations with four variables and apparently look very complicated. Equations (2.3b–d) which describe the dynamics of gating variables, however, share a simple common structure. Functions $\tau_x(v)$ and $x^\infty(v)$, $x = m,n,h$ depend on the membrane potential v and thus vary temporally with the temporal change of v. If we assume that the functions do not depend on v ($\tau_x(v) \equiv \tau_x$, $x^\infty(v) \equiv x^\infty$), then (2.3b–d) reduce to a linear differential equation

$$\frac{dx}{dt} = \frac{1}{\tau_x}(x^\infty - x), \quad x = m,n,h,$$

whose analytical solution with an initial value $x = x_0$ is

$$x(t) = \exp(-t/\tau_x)(x_0 - x^\infty) + x^\infty.$$

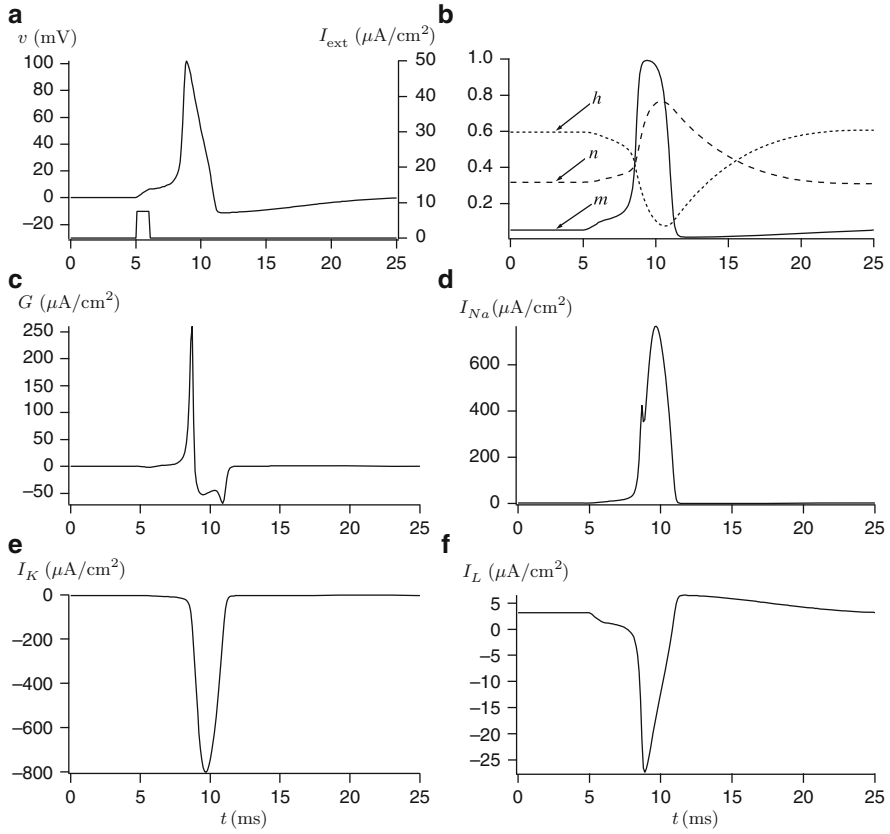

Fig. 2.4 Solution of the Hodgkin–Huxley equations

The variable $x(t)$ approaches x^∞ at a speed depending on a time constant τ_x. In (2.3b–d), although they are function of v and we cannot solve the equation analytically, $\tau_x(v)$ still preserves a role of "time constant" and $x^\infty(v)$ is the steady-state function to which the variable x asymptotically approaches in a steady (or stationary) state.

Figure 2.5a shows the functions $x^\infty(v),\ x = m, n, h$. In spite of the complicated functional forms, these functions are all monotonic functions and have the shape of so-called "sigmoid function." $m^\infty(v)$ and $n^\infty(v)$ are increasing functions and thus variables m and n are activation variables while $h^\infty(v)$ is a decreasing function and h is an inactivation variable. Figure 2.5b shows the functions $\tau_x(v),\ x = m, n, h$ which change depending on v. The function $\tau_m(v)$, however, much smaller than $\tau_n(v), \tau_h(v)$ in the whole range of v. In the following, let us explore the dynamics of the HH equations regarding this time-scale difference.

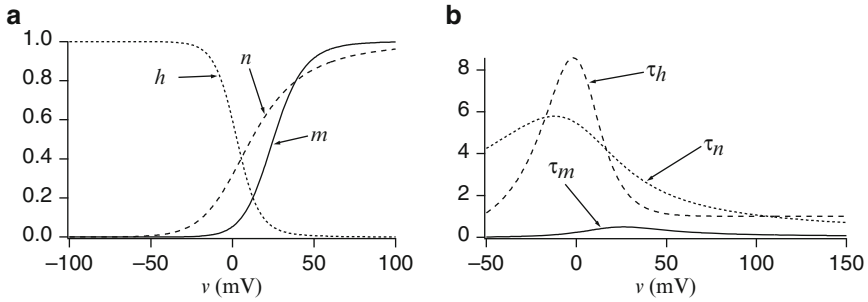

Fig. 2.5 Various functions in the Hodgkin–Huxley equations

2.3.2 FitzHugh's Subsystem Analysis of the HH Equations

In this subsection, following the pioneering paper FitzHugh (1960), let us see from what dynamics the threshold property of a neuron or the HH equations comes. The HH equations have four variables and it is difficult to observe the full (four-dimensional) state space directly. The separation of the full state space to several subspaces, however, resolves this difficulty. As shown in Fig. 2.5, the "times constants" of variables n and h are much bigger than that of m; n and h change their values more slowly than m. Thus we (temporarily) ignore the dynamics of n and h in the HH equations and consider the following system:

$$C\frac{dv}{dt} = \bar{g}_{\mathrm{Na}}m^3h(V_{\mathrm{Na}} - v) + \bar{g}_{\mathrm{K}}n^4(V_{\mathrm{K}} - v) + \bar{g}_{\mathrm{L}}(V_{\mathrm{L}} - v), \tag{2.5a}$$

$$\frac{dm}{dt} = \frac{1}{\tau_m(v)}(m^\infty(v) - m). \tag{2.5b}$$

(We call this system as the v–m subsystem.) In the v–m subsystem, v and m are the dynamic variables while h and n are set in suitable values as a "parameter."

By using the v–m subsystem, let us explain the firing process in the HH equations in the following order:

quiescent state → depolarization → decrease of h → increase of n → repolarization .

Figure 2.6a shows the v–m phase plane of (2.5) when the values of h and n are fixed to that of the quiescent state (a stable equilibrium point) of the HH equations (2.3). The m-nullcline (a curve in which $dm/dt = 0$: $m = m^\infty(v)$) is a sigmoidal monotonically increasing function. (For more explanation of nullclines, see Chap. 3.) We can see that the v-nullcline (dotted curve) and m-nullcline (solid curve) intersect in the three points v_1^*, v_2^* and v_3^* which are equilibrium points of the v–m subsystem (panel b is the magnification of lower-left region of a). The leftmost equilibrium

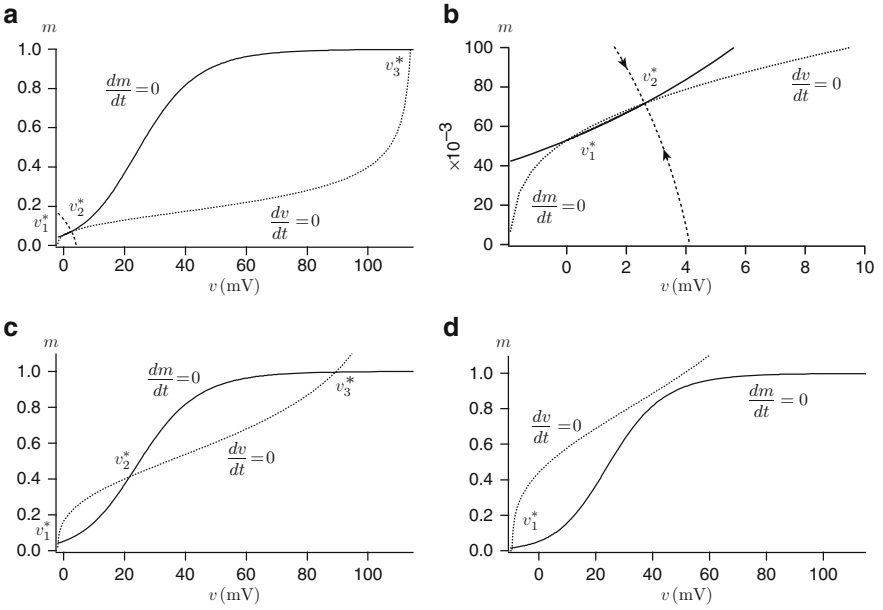

Fig. 2.6 Phase plane of the v–m subsystem (2.5) of the HH equations. (**a**) $n = 0.317677$, $h = 0.596120$. (**b**) Magnification of (a). (**c**) $n = 0.317677$, $h = 0.02$. (**d**) $n = 0.5$, $h = 0.02$

point v_1^* corresponds to the quiescent state (a stable equilibrium point) and the middle point v_2^* is a saddle point whose stable manifold (the broken curve tending to v_2^*) forms a threshold between exciting and non-exciting, which means that the HH model when h and n are fixed to the values of quiescent state is the type-I neuronal model with a strict threshold. If a sufficiently large stimulus is applied to a neuron in a quiescent state v_1^*, the state point moves rightwards beyond the stable manifold of v_2^* and then goes towards the rightmost equilibrium v_3^* which corresponds to the depolarized state of a neuron. If a membrane potential v increases, h is decreased (after a slight delay) because the variable h tends to the function $h^\infty(v)$ which is a decreasing function of v.

Figure 2.6c is the phase plane with a smaller value of h. In the v–m subsystem (2.5), the v-nullcline does depend on both h and n while the m-nullcline does not depend on them. From (2.5a), the v-nullcline is obtained by

$$m^3 = \frac{\bar{g}_{\mathrm{K}} n^4 (v - V_{\mathrm{K}}) + \bar{g}_{\mathrm{L}} (v - V_{\mathrm{L}})}{\bar{g}_{\mathrm{Na}} h (V_{\mathrm{Na}} - v)} \tag{2.6}$$

from which we can see that the decrease of h moves the v-nullcline upward (the shape of v-nullcline is also changed). Note that we consider this equation in the range of $0 \leq m \leq 1$, thus the right-hand side is positive. As a result of displacement of the v-nullcline, three intersections of the v-, m-nullclines become more clearly

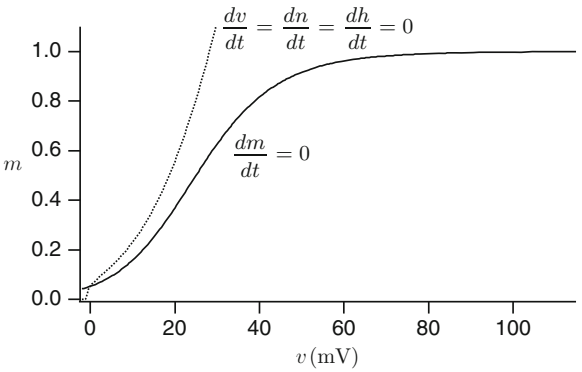

Fig. 2.7 v–m Phase plane of the HH equations (2.3)

distinguishable. As is seen from Fig. 2.5b, in the depolarized (high-voltage) region of v, $\tau_n(v)$ is slightly larger than $\tau_h(v)$. Thus n increases subsequently to the decrease of h (practically, these changes occur almost simultaneously) since $n^\infty(v)$ is a increasing function of v.

Figure 2.6d shows the case that n is increased in addition to the decrease of h. As is seen from (2.6), the further increase of n moves the v-nullcline upward. Then two equilibria v_2^* and v_3^* disappear by a saddle-node bifurcation and only equilibrium v_1^* remains. As a result of disappearance of those equilibria, the state point near the equilibrium v_3^* (depolarized state) cannot stay there and then changes its direction toward the equilibrium v_1^* (quiescent state). After this process, h and n change to increase and decrease, respectively, and then return to the state of Fig. 2.6a.

Figure 2.7 shows the v–m phase plane of the *full* HH equations (2.3) (projection of the four-dimensional state space to v–m phase plane). The sigmoid-like curve is the m-nullcline and is same as the case of v–m subsystem. The other curve denotes the intersection of v, n, h-nullclines; a curve such that $dv/dt = dn/dt = dh/dt = 0$:

$$m^3 = \frac{\bar{g}_\mathrm{K}\{n^\infty(v)\}^4(v - V_\mathrm{K}) + \bar{g}_\mathrm{L}(v - V_\mathrm{L})}{\bar{g}_\mathrm{Na}h^\infty(v)(V_\mathrm{Na} - v)}.$$

The intersection of these two nullclines corresponds to the equilibrium point of the original HH equations (2.3) and thus the HH equations have a unique equilibrium. This implies that in a strict sense the original HH equations are a type-II neuronal model without a distinct threshold. As is seen above, however, in a very short time range (i.e. if we ignore the temporal change of h and n) the HH equations behave like a type-I neuronal model which has a distinct threshold. Thus we can understand why the HH equations have a relatively sharp threshold although they do not have any threshold in a strict sense.

2.3.3 Dynamic I–V Relation of the Squid Giant Axon Membrane

In this subsection, let us investigate the HH equations from more global viewpoint without entering into its detailed dynamics. Figure 2.8 shows dynamic or transient current–voltage relation of the HH equations; total membrane currents G when a time t elapses after the membrane voltage is instantaneously changed to v (mV) from the quiescent state are plotted for various v values. These current–voltage relations are shown for various values of the time t. At a time $t = 0.02$ ms, the relation is almost linear. After some time elapses, negative-resistor characteristics appear and the current–voltage relation becomes N-shaped. After sufficiently long time elapses, the relation shows a rectifier characteristics in which only outward current can be flowed.

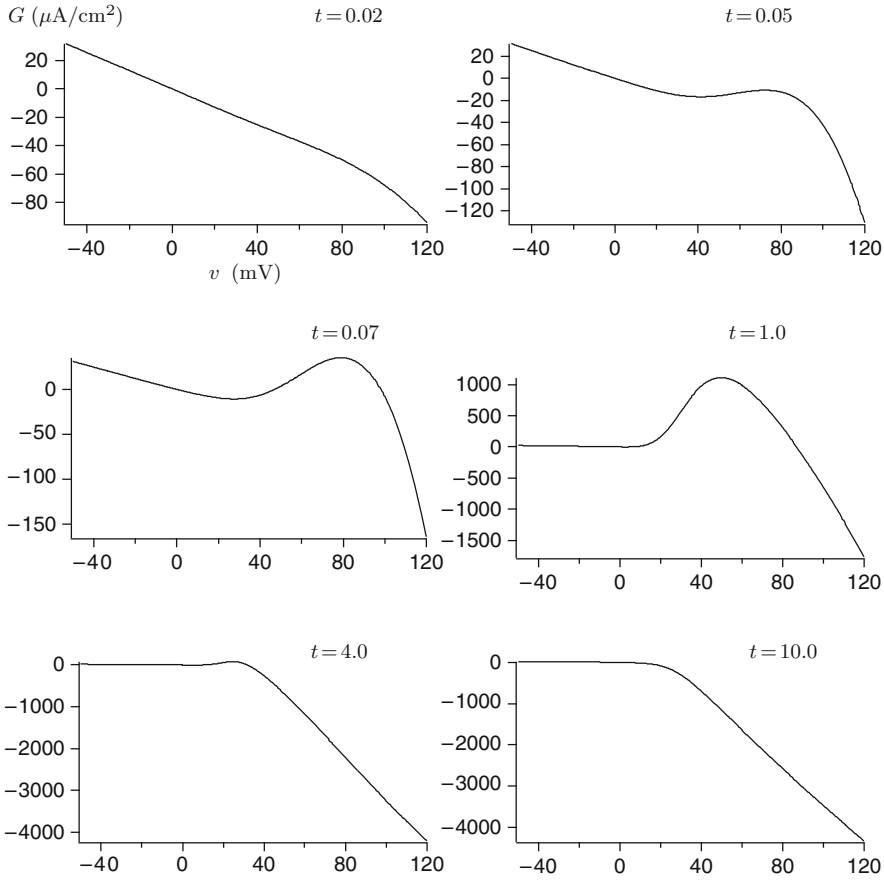

Fig. 2.8 Transient current–voltage relations of the Hodgkin–Huxley membrane

In order to see how these current–voltage relations are generated, let us decompose the total membrane current to its components: I_{Na} and I_{K} where the (small) leak current is ignored. Figure 2.9 is the similar voltage–current relations to Fig. 2.8 for Na and K channels. When $t = 0.02$, the relation of K channel (dotted curve) is almost linear. After time elapses, the K current in a low-voltage range becomes small and finally, the current–voltage relation becomes a rectifier. In the case of Na channel (solid curve), when $t = 0.02$, it does not flow much current (almost flat). After suitable time elapses, it shows large nonlinear characteristics and then finally becomes almost flat again. The combination of these two current–voltage relations makes the I–V relation of the total current in Fig. 2.8.

The above current–voltage relations are obtained by numerically solving the HH equations (2.3). The relation when $t = 10.0$ is considered as a steady-state current–voltage relation. This relation can be obtained directly (without numerical simulation) from the HH equations (2.3) as

$$G(v, m^{\infty}(v), n^{\infty}(v), h^{\infty}(v)).$$

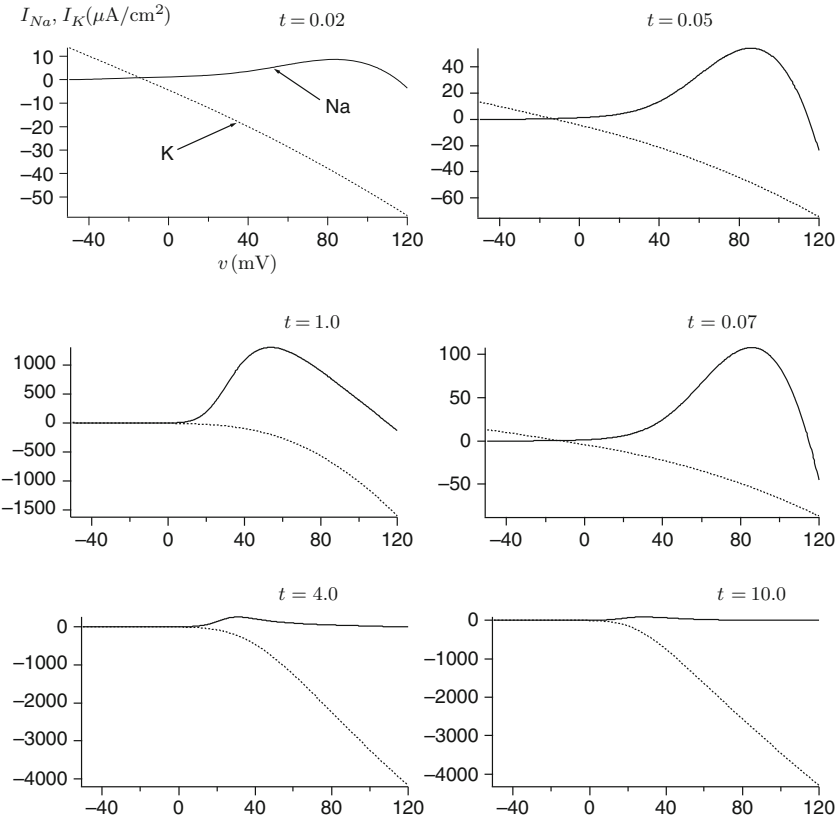

Fig. 2.9 Transient current–voltage relations of Na and K channels

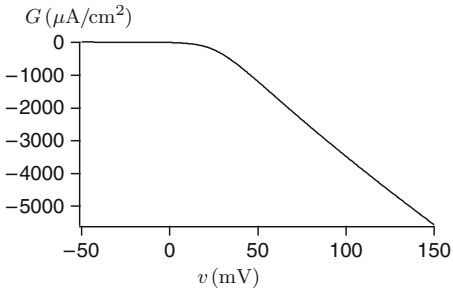

Fig. 2.10 Steady-state current–voltage relation of the Hodgkin–Huxley equations

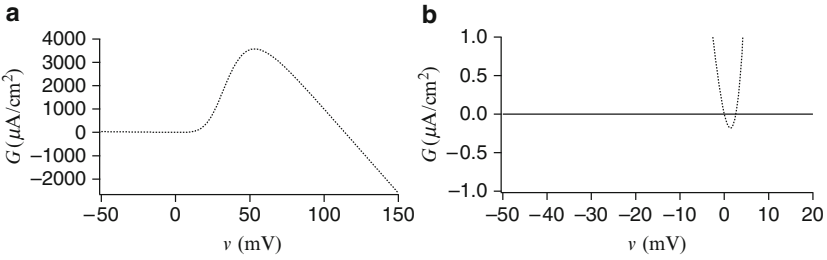

Fig. 2.11 (**a**) Steady-state current–voltage relation of the v, m-subsystem of the HH equations. (**b**) Magnification of (a)

This steady-state current is plotted as a function of v in Fig. 2.10. Similarly to the $t = 10$ case of Fig. 2.8, we can see the rectifier characteristics.

Figure 2.11 shows the steady-state current of the v–m subsystem (2.5):

$$G(v, m^{\infty}(v), n^*, h^*)$$

as a function of v where n^* and h^* denote the quiescent-state values of n and h, respectively. Panel (b) is the magnification of (a), from which the current–voltage curve intersect with the horizontal line at three points which correspond to the three equilibrium points of the phase plane of Fig. 2.6a. From this observation, we can also see the threshold property of the HH equations.

Comparing Fig. 2.11 to the transient current–voltage relation of Fig. 2.8, we confirm that the v–m subsystem approximates the dynamics of the full HH equations (2.3) in the time scale of $t \leq 1$ ms.

2.3.4 Dimension Reduction of the HH Equations

In the v–m subsystem analysis, we investigated the v–m phase plane of the HH equations by fixing the values of n and h. Namely, we explored the dynamics of HH equations by decomposing the four-dimensional full phase space into several n, h-fixed slices.

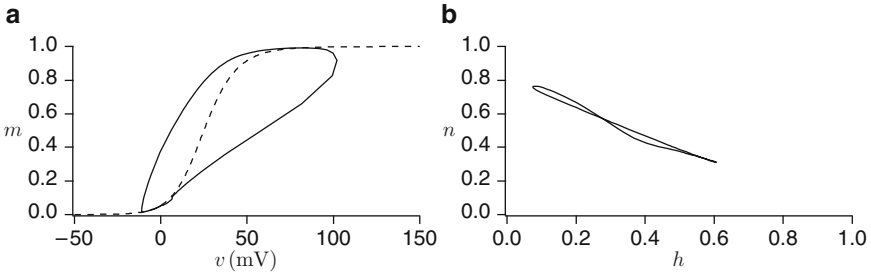

Fig. 2.12 Projections of the orbit (solution) of the HH equations to (**a**) a v–m phase plane and to (**b**) a h–n phase plane

This subsection briefly describes the method which reduces the full four-dimensional system into two-dimensional system (FitzHugh 1961; Krinskii and Kokoz 1973; Kokoz and Krinskii 1973; Rinzel 1985). Although such dimension reduction, differently from the v–m subsystem analysis, loses some information on original dynamics, it is useful to catch the essential feature of the whole four-dimensional dynamics of the HH equations on a reduced phase plane.

Figure 2.12 shows the projections of an orbit (solution) $(v(t), m(t), h(t), n(t))$ of the HH equations to (a) a v–m phase plane and to (b) a h–n phase plane. From panel (a), we can see that the orbit in the region of $m \approx 0$ or $m \approx 1$ moves close to the m-nullcline $m = m^{\infty}(v)$ (broken curve). Panel (b) shows that the orbit moves restricted in a certain line on the h–n phase plane.

From these observations, we reduce the HH equations (2.3) in two steps:

1. Suppose that the variable m which follows (2.3b) is settled in its steady-state value: $m = m^{\infty}(v)$ since m is the fast-changing variable (τ_m is small). Thus we ignore (2.3b) and substitute $m^{\infty}(v)$ for m in (2.3a).
2. Approximate the orbit on the h–n phase plane by a line $n = 0.8(1 - h)$; we consider that the variable n linearly depends on h. Thus we ignore (2.3c) and substitute $0.8(1 - h)$ for n in (2.3a).

From these reduction steps, we obtain the reduced equations:

$$C\frac{dv}{dt} = G(v, m^{\infty}(v), 0.8(1-h), h) + I_{\text{ext}}, \tag{2.7a}$$

$$\frac{dh}{dt} = \alpha_h(v)(1-h) - \beta_h(v)h. \tag{2.7b}$$

This model has only two dynamic variables v and h, and thus has an advantage that we can analyze the neuronal dynamics on a phase plane rather than the four-dimensional phase space of the original HH equations.

Figure 2.13a shows an example of the membrane potential waveforms of the original HH equations (2.3) (dotted curve) and of the reduced model (2.7) (solid curve). The upstroke of the membrane potential of the reduced model is slightly faster than that of the HH equations and the peak value is also bigger than the HH equations.

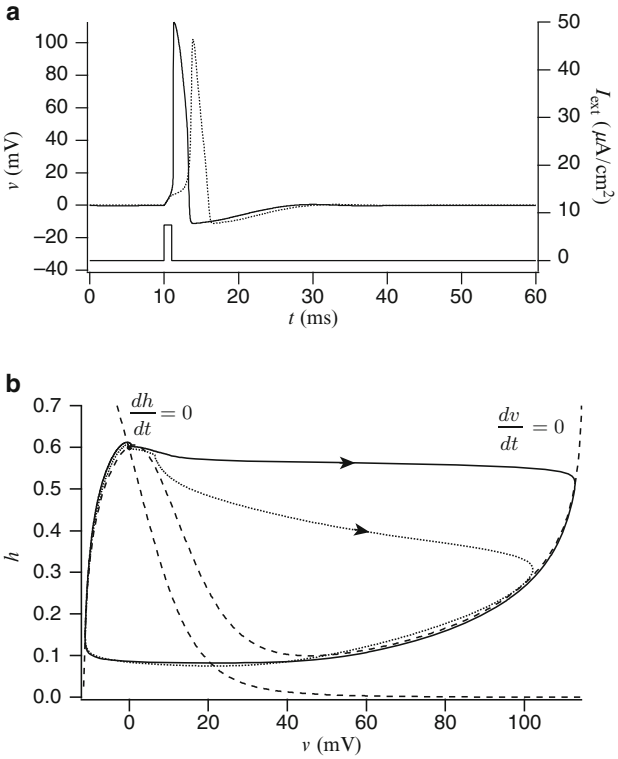

Fig. 2.13 Comparison of **(a)** membrane potential waveforms and **(b)** solution orbits in the phase plane, between the dimension-reduced model (*solid curve*) and the original HH model (*dotted curve*)

This is because we substituted $m^{\infty}(v)$ for m and thus the activation process of Na channel has been slightly accelerated. Except for these small differences, the two waveforms of the original and the reduced model are quite similar. This similarity is surprising since the dimensions of the original and the reduced model are much different.

Figure 2.13b shows the solution orbit of both models on the v–h phase plane. The solid curve denotes the orbit of the reduced model (2.7), and the dotted curve the original HH equations (2.3). The v-nullcline

$$G(v, m^{\infty}(v), 0.8(1-h), h) = \bar{g}_{\mathrm{Na}}(m^{\infty}(v))^3 h(V_{\mathrm{Na}} - v) + \bar{g}_{\mathrm{K}}(0.8(1-h))^4(V_{\mathrm{K}} - v) + \bar{g}_{\mathrm{L}}(V_{\mathrm{L}} - v) = 0$$

and the h-nullcline

$$h = h^{\infty}(v) = \frac{\alpha_h(v)}{\alpha_h(v) + \beta_h(v)}$$

are also shown by broken curves. We can see the similarity of orbits of the two models except for the slight difference in the action potential upstroke.

Topological features (one nullcline is N-shaped and the other is monotonic) of the phase plane of the reduced model resemble to that of the Bonhoeffer–van der Pol (BVP) or FitzHugh–Nagumo (FHN) model (FitzHugh 1961; Nagumo et al. 1962). In fact, the assumptions (i) and (ii) which are used to derive the reduced model (2.7) (Krinskii and Kokoz 1973; Rinzel 1985) is essentially the same as the one used by FitzHugh to derive the BVP model (FitzHugh 1961). The reduced model (2.7) by Krinskii and Kokoz (1973) and by Rinzel (1985) is derived by some logical process while the BVP model is derived a priori. Thus, the relation of physiological parameters of the original and the simplified models are much clear in the model (2.7) rather than in the BVP model. For more systematic reduction of general HH-type models, see Abbott and Kepler (1990), Golomb et al. (1993), and Kepler et al. (1992).

2.3.5 *Bifurcation Analysis*

In this subsection, we consider the dependence of the HH equations' behavior on the parameter I_{ext}; the constant-current-transfer characteristic of the HH neuron (Rinzel 1978; Guttman et al. 1980). The neuron model produces an action potential with response to an external pulsatile stimulus. We can expect that the neuron generates action potentials persistently when a continuous current is applied externally.

Figure 2.14 shows the example of such repetitive firings (oscillation or periodic orbit) of the HH neuron when $I_{\text{ext}} = 7$. At $t = 62$, a pulsatile stimulus is applied to the neuron in addition to the constant current injection. After the pulse stimulus, the repetitive firing is stopped in spite of the persistent injection of the constant current. This means that an repetitive firing (stable limit cycle) and a quiescent state (stable equilibrium) coexist when $I_{\text{ext}} = 7$. The state point of the HH neuron is moved from one attractor (limit cycle) to an another one (equilibrium) by the external pulse.

We note that the applied pulse is depolarizing current; not only inhibitory input but also excitatory input can inhibit such repetitive firing since it is a nonlinear oscillation. The timing (phase) when the pulse is applied is important.

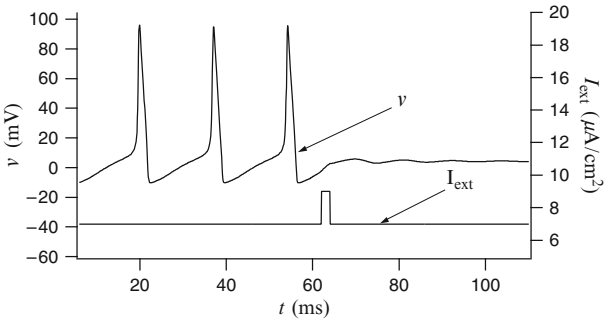

Fig. 2.14 Example of a membrane potential waveform of the HH equations when an external constant current is applied: $I_{\text{ext}} = 7\,\mu\text{A cm}^{-2}$. A pulse is applied to the model in addition to the constant current at $t = 62$

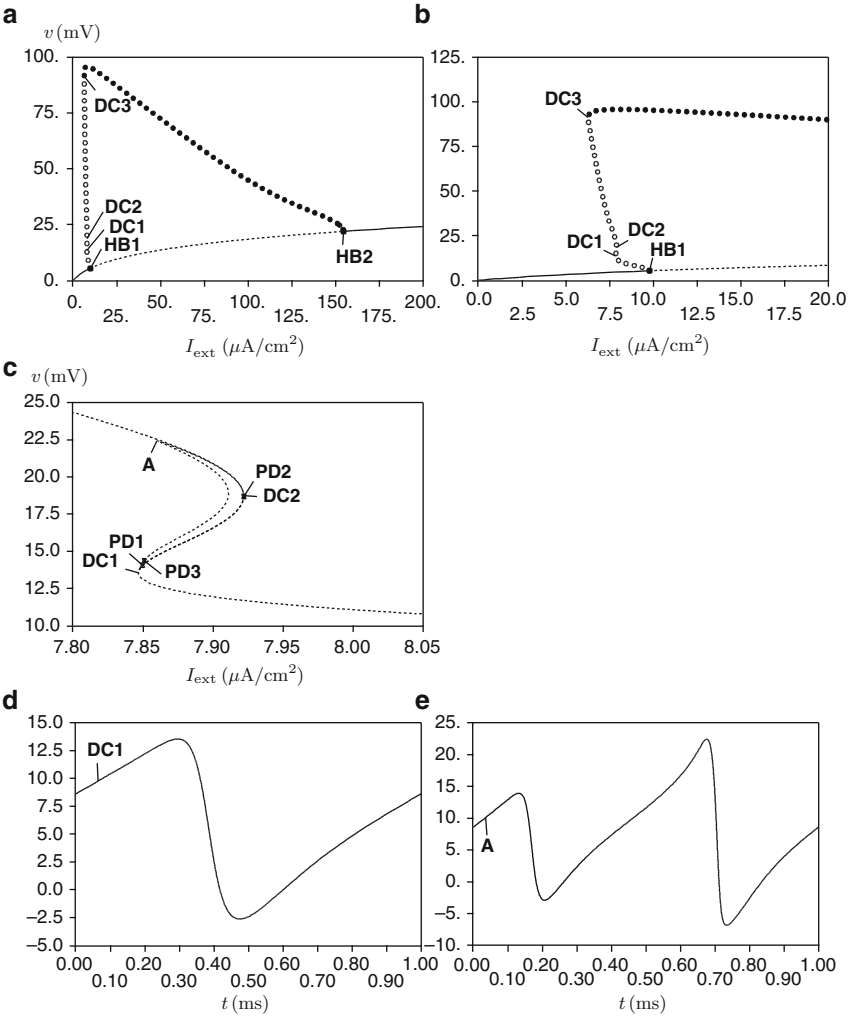

Fig. 2.15 (**a**) One-parameter bifurcation diagram of the HH equations. (**b**) Magnification of (a). (**c**) Magnification of (b). (**d**, **e**) Membrane potential waveforms at the points `DC1` and `A` of (c)

Figure 2.15a shows the dependence of the solution of the HH equations on the parameter I_{ext}; the v values of the stationary solution of the HH equations are plotted for various values of I_{ext} where the maximum value of v is plotted for a periodic (oscillatory) solution. Solid and dotted curves denote stable and unstable equilibria, respectively. The filled (open) circles denote stable (unstable, resp.) periodic solutions.

Panel (b) is the magnification of left part of (a) and we can verify the multistability of an equilibrium and a periodic solution when $I_{ext} = 7$ (ref. Fig. 2.14). At the point `HB2` of panel (a), a stable periodic solution bifurcates from a equilibrium point by the (super-critical or stable) Hopf bifurcation. An unstable periodic solution

is bifurcated by the (sub-critical or unstable) Hopf bifurcation at the point HB1. As is seen from panel (b), a multistability occurs near the sub-critical Hopf bifurcation. At the point DC3, a double-cycle bifurcation or saddle-node bifurcation of periodics occurs and a pair of stable and unstable periodic solutions is generated.

At both points DC1 and DC2, double-cycle bifurcations occur also. Near $I_{\text{ext}} = 7.9$, four periodic solutions (one stable solution and three unstable solutions) coexist (Rinzel and Miller 1980). The fact is that there are more coexisting (unstable) solutions. Panel (c) is the magnification of the region near the points DC1 and DC2 of (b). (Note that the periodic solutions are denoted by curves rather than circles.) At the points PD1 and PD2, period-doubling bifurcations of unstable periodic solution occur. Panel (d) shows the membrane potential waveform (only one-period length of periodic solution is shown and abscissa is the time normalized by its period) of such unstable periodic solution at the point DC1 of panel (c). Panel (e) is the similar waveform of the period-doubled solution at the point A of panel (c).

We can not observe such unstable solutions in real experiments. The unstable solutions, however, connect "the missing links" between stable solutions and much help us to understand the total behavior of neuronal models. The bifurcation analysis of Fig. 2.15 is made by the use of numerical bifurcation analysis software called AUTO (Doedel et al. 1995). AUTO is very useful software which can detect several bifurcation points automatically and can trace both stable and unstable branches of equilibria and periodic solutions.

Figure 2.16a shows the period of the periodic solutions shown in Fig. 2.15a. Panel (b) is the magnification of panel (a). The period of stable periodic solutions (closed circle) varies in the range from several milliseconds to 20 ms. The period does not change much totally although the variation is comparatively large in the small I_{ext} range.

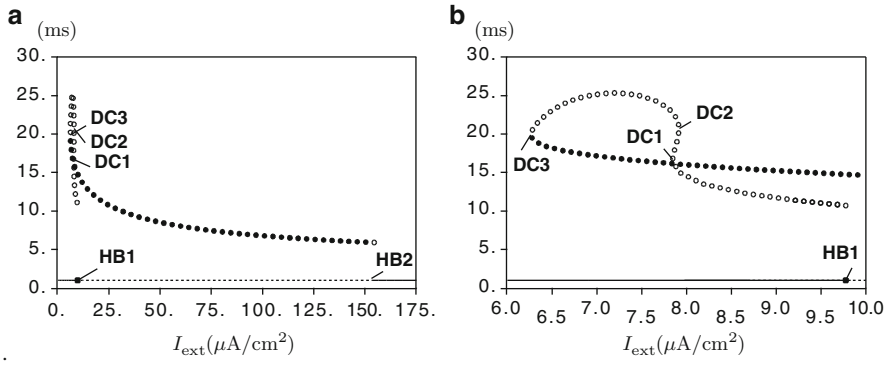

Fig. 2.16 (**a**) Period of the periodic solution shown in Fig. 2.15a and (**b**) Magnification of (a)

http://www.springer.com/978-4-431-53861-5

Computational Electrophysiology

Doi, S.; Inoue, J.; Pan, Z.; Tsumoto, K.

2010, 140 p., Softcover
ISBN: 978-4-431-53861-5